LAWRENCE
LIVERMORE
NATIONAL
LABORATORY

LLNL-JRNL-654750

Parameter Study of an Inertial Fusion Energy Chamber Response using the 1-D BUCKY Radiation Hydrodynamics Code

R. Sacks, G. Moses, V. Tang, K. Kramer, H. Scott, J. DeMuth

May 23, 2014

Fusion Science and Technology

Disclaimer

PARAMETER STUDY OF AN INERTIAL FUSION ENERGY CHAMBER RESPONSE USING THE 1-D BUCKY RADIATION HYDRODYNAMICS CODE

Ryan Sacks,[a*] Gregory Moses,[a] Vincent Tang,[b]
Kevin Kramer,[b] Howard Scott,[b] James DeMuth[b]

[a]Fusion Technology Institute, University of
Wisconsin-Madison, Madison, Wisconsin, 53706

[b]Lawrence Livermore National Laboratory,
Livermore, California, 94550

[*]rsacks@wisc.edu, 1500 Engineering Drive Room 410
Madison WI, 53706, 269-598-3089

Figures: 11, Tables: 4, Pages: 33

April 25, 2014

Abstract

PARAMETER STUDY OF AN INERTIAL FUSION ENERGY CHAMBER RESPONSE USING THE 1-D BUCKY RADIATION HYDRODYNAMICS CODE

Ryan Sacks,[a*] Gregory Moses,[a] Vincent Tang,[b] Kevin Kramer,[b] Howard Scott[b] and James DeMuth[b]

[a]Fusion Technology Institute, University of Wisconsin-Madison, Madison, Wisconsin, 53706

[b]Lawrence Livermore National Laboratory, Livermore, California, 94550

[*]rsacks@wisc.edu, 1500 Engineering Drive Madison WI, 53706, 269-598-3089

A parameter study of a proposed inertial fusion energy chamber is performed. A baseline case of a 6 meter radius chamber filled with 6 μg/cm^3 of xenon is studied in detail. The maximum first wall temperature is shown to be 1136 K with an overpressure of 5.83×10^{-3} MPa. A parameter sweep is conducted for the chamber by adjusting the first wall radius from 4 to 14 meters, changing the gas density and by changing the fill gas from xenon to argon. The results set limits on first wall radius for different gases and densities. Analytic fits to simulation results allow their use in overall engine design tradeoff studies.

Keywords: *Inertial Confinement Fusion, Inertial Fusion Energy, Radiation Hydrodynamics*

I Introduction

Inertial fusion energy reactor conceptual designs are commonly described by the type of driver, the type of target and the mechanism used to protect the plasma facing surface in the reactor chamber, sometimes called the nuclear island or the fusion engine. Driver types are heavy ion beam accelerators[1][2][3], lasers[4][5][6][7][8] and pulsed power systems[9]. Targets are categorized as either spherical direct drive targets that are illuminated uniformly over their surface by uniformly positioned driver beams (SOLASE[1], High Average Laser Power (HAPL)) or indirect drive targets where driver beams are clustered, usually entering ends of the target cylindrical hohlraum from two directions in narrow cones of beams (SOLASE, High-Yield Lithium-Injection Fusion Energy (HYLIFE), Heavy Ion Beams and Lithium Lead (HIBALL), Laser Inertial Fusion Energy (LIFE)). The design feature used to protect the first plasma facing surface is important because the impulsive nature of the energy release from an exploding inertial fusion target can damage the first wall. Therefore various mechanisms have been proposed to protect the surface from this impulsive heat loading. Inclusion of streaming liquid metal jets between the exploding target and the first wall (HYLIFE, HIBALL), introduction of a low pressure gas in the fusion engine chamber (SOLASE, LIFE) or simply sizing the chamber with a radius sufficiently large to increase the sur-

[1] As in the following quote: "[...]their **solase** in dorckaness, and splattering together joyously the plaps of their tappyhands as, with a cry of genuine distress, so prettly prattly pollylogue, they viewed him, the just one, their darling, away." J. Joyce, Finnegans Wake, The Viking Press, New York (1939), p.470

face area to the point that the peak heat flux is manageable are three common mechanisms to protect the first wall (HAPL).

The specific inertial fusion energy (IFE) reactor parameter underlying the analysis in this paper are given in Table I[10]. In this design, indirect drive fusion targets are injected into the fusion chamber at a rate of 16 per second and produce a total yield of 132 MJ with approximately 74% of the energy carried by neutrons, 13% emitted as x-rays and the remaining 13% in the expanding ions. The chamber is filled with 0.845 torr[2] of gas and this is allowed because the indirect drive target hohlraum serves as the thermal shield as the target is injected into the hot chamber. Laser propagation through the gas is of concern as attenuation or wave front distortion of the laser beam might adversely affect the amount of energy delivered to the target and the absorption processes. Research on this topic shows that very diffuse gas fills of the chamber lead to a negligible degradation of laser performance[13]. The x-ray spectra for the target (see Figure 3) is generated by the Lasnex code at Lawrence Livermore National Laboratory (LLNL), fit to 3 Planckian distributions and then input into the BUCKY radiation hydrodynamics code[11][12]. The neutrons, mostly at 14.1 MeV have little effect on the gas dynamics of the chamber and are assumed to stream into a blanket layer where they are thermalized, captured, and converted to usable energy and tritium. The possibility of running the engine as a fusion-fission hybrid that utilizes the high

[2]The value of 0.845 torr value is arrived at by calculating the ideal gas pressure at 293 K for the specified density of 6 $/mu$g/cm^3. Historical literature often quotes gas density in terms of pressure.

energy neutrons to breed fissile material along with producing tritium has also been studied[14].

The gas filled chamber design shields the first wall from direct bombardment by the target ions and attenuates the prompt x-rays from the target. This allows the first wall radius to be much reduced from that of a near vacuum chamber as in the HAPL design. The ions deposit their energy in approximately 100 cm in the gas, generating an initial blast wave in the xenon that propagates outward to the chamber wall while the thickness of the gold hohlraum is assumed to be enough to stop the 3.5 MeV alpha particles. The range of 3.5 MeV alphas in gold is $11 \times 10^{-3} g/cm^2$, this requires a thickness of between 5.7-11 microns[15]. In simulations, the x-ray spectrum is modeled as 121 logarithmically spaced energy groups from 0.1 to 100 keV. The unattenuated x-rays produce a prompt temperature response on the first wall surface and the attenuated x-rays produce a Marshak heat wave that propagates through the Xe gas. These dynamics are affected by a number of variables designated in the chamber design; chief among them are chamber radius, chamber fill gas and fill gas density. All of these properties are easily manipulated in computer simulations and give bounds on the design of the chamber. Differing fill gases will affect the shock speed of the initial blast wave produced by the deposition of the energy in the ions. The purpose of these 1-D simulations is to estimate the conditions of the gas filled chamber and first wall material after multiple fusion events. This allows for consideration of the materials used for both the fill gas and the first wall.

These results well characterize bounds for the engine fill and radius, but must be taken as a 1^{st} approximation due to the lack of a turbulence model and consideration of multi-dimensional hydrodynamic effects.

II Radiation Hydrodynamics Model

The BUCKY code is a 1-D lagrangian radiation hydrodynamics code under development since 1973. It models plasmas using the one fluid, two temperature (electron and ion) approximation.Equations of state from a number of sources including SESAME, Flexible Atomic Code (FAC) and University of Wisconsin equation of state codes[16][17][18] are compatible with BUCKY. It models radiation using multi-group flux-limited diffusion theory. BUCKY uses group-wise opacities from a number of sources including FAC and UW opacity codes and has full capability of modeling target implosions and thermonuclear burn, including burn product energy deposition. It has energy input models for lasers (including ray tracing), ions and electron beams. More important to this paper is BUCKY's capability to model stationary solid state materials with table inputs for thermal conductivity, specific heat, and melting and vaporization temperatures. This allows accurate thermal modeling of the chamber first walls. Simulating target explosions in gas filled chambers is a unique capability of BUCKY. The target explosion is modeled as a point x-ray and ion source at the center of a spherical chamber. X-ray source terms are input into BUCKY

as time and energy dependent data tables. Ion source terms are input into BUCKY as time, energy, and species dependent data tables.

III Base Case Analysis

The base case is defined as a 6 meter radius chamber filled with xenon gas with a density of 6 μg/cm^3 with an initial temperature of 0.45 eV (see Table I for details on simulation set-up and for a model see Figures 1 and 2). The initial temperature was determined by running the base case simulation to estimate a cyclic steady state by taking the final time zone boundaries, ion, electron and radiation temperatures and densities as the initial conditions for the next simulation. The final cyclic steady state temperature is approximated by taking a mass average of the temperatures across the zones. The x-ray source term has a Gaussian temporal distribution with a total emission time of 35 ns. All energies are distributed in time with only the intensity of each group varying as given by Figure 3. The ion spectra is shown in Figure 4 and like the x-ray spectra is released as a point source at the chamber center. Here ions are given a kinetic energy and allowed to slow down and deposit energy into the gas via the expected ion stopping power relations. This case is examined to set a baseline for the temperature rise in the first wall, speed of shock wave propagation and effect of the Marshak wave dynamics on the chamber state. The number of finite dif-

ference zones used to describe the gas is tested to investigate the effect on convergence of outputted quantities. In all cases, for the gas zone test described in this section and the parameter study done in the later sections, the same number of zones are used in the wall to allow for comparison of the same wall response with differing chamber parameters.

III.A Zone Refinement and Results

In each case there are 70 zones in the wall. The first 30 of the wall zones are chosen by estimating the discretized thermal time constant of the wall material:

$$\Delta t = (\frac{\rho C_v}{\kappa})(\Delta x)^2 \tag{1}$$

Which can be rearranged to:

$$\Delta x = \sqrt{\frac{\kappa}{\rho C_v}\Delta t} \tag{2}$$

where Δt is the characteristic time in seconds defined in the input for the prompt x-ray emission, in this case 1×10^{-13} seconds. Equation 2 requires the first wall surface zone to be 7×10^{-8} cm thick. Using this value, the total 70 zones of the wall are divided into two sections: 30 zones that are all 7×10^{-8} cm and 40 zones that increase in thickness from zone to zone by 38.5 % to bring the wall up to a total thickness of 0.11 cm. This is done in to increase the accuracy of the thermal gradient in the first wall. This gradient is extremely steep as the wall heats up (see Figures 8 and 11) The wall material used in all cases is 409

stainless steel[2] with material properties taken from the product data bulletin from the AK Steel Corporation[20]. The properties of the steel are plotted in Figure 5 and for any temperatures that are off scale are extrapolated.

The zone numbers in the gas used to study the effect on the chamber dynamics are 250, 400 and 600. In each case, the first zone is 28.8 cm, which with the 6 μg/cm^3 of xenon gas fill is 1 gram of material. This is chosen since the hohlraum target is constructed of approximately 1 gram of lead, leading the first zone to have the same mass as a target. Each simulation is followed by a region of zones of increasing width (150, 300 and 500) with the last 100 zones not increasing. The simulation is run for 62.5 ms, the time between shots for the engine operating at 16 Hz. The results of these simulations show that the maximum first wall temperature in the first zone of the wall is the same, 1136 K, and the maximum overpressure is similar in all cases, varying only slightly between the 400 zone case and the 600 zone case by 4×10^{-5} MPa (5.83×10^{-3} and 5.87×10^{-3} MPa)and the 250 zone case only varying by 5×10^{-5} MPa (5.78×10^{-3} MPa). Additionally, in each case an outer shock arrives at the wall at 2.4 ms with an inner shock arriving at 4.25 ms (this can be seen in the RT plot given in Figure 6). As each case has nearly identical output, all subsequent simulations for the parameter study are done with 400 zones in the gas.

[2]While these simulations are performed with 409 stainless steel as a representative wall material, the engine will use HT-9 to reduce neutron activation[19].

III.B Double Shock

Clearly seen in Figure 6 are two distinct shocks incident on the wall at different times. The inner shock forms at about 100 cm from chamber center and is created from slowing down and stopping of the expanding target ions by the gas. The outer shock forms at about 320 cm from chamber center and is created from the Marshak wave slowing to approximately the fluid response time of the gas. This is revealed by the time sequence of the Marshak wave as it propagates through the gas (see Figure 7). This outer shock, which arrives at the wall first is seen in all simulations carried out in this parameter study, and when the Marshak wave is plotted as it is in Figure 7 for the given gas fill and density, it has a similar shape and stalls at around the same radius that the outer shock develops. The two shock phenomenon deserves further study.

IV Parameter Study

The main aim of the parameter sweep is to investigate what effect the fill gas type, fill gas density and chamber radii have on the chamber and first wall response to target explosion. Splitting the parameters into two groups, gas fills and chamber radii, simulations are run with radii of 4, 5, 6, 8, 10, 12 and 14 meters and gas fills of xenon at 6 and 2 μg/cm^3 and argon at 6 and 1.86 μg/cm^3. The value of 1.86 μg/cm^3 is chosen as this is the same number density of xenon at 6 μg/cm^3. The three main engineering design quantities of interest for each simulation are

maximum first wall temperature, maximum overpressure on the first wall and arrival of shock wave(s) at the first wall. The first wall temperature is key because as a thermo-electric power plant, the higher the first wall temperature the more efficiently electricity can be generated[10]. In addition to the generation of electric power, the maximum temperature of the first wall must be determined to ensure that the candidate materials can survive. To this end a temperature of 2/3 the melting temperature of the surrogate steel is considered the design limit. This temperature, 1202 K, is compared with the first wall temperatures of each case. The base case mentioned in Section 2 is 66 K lower than this limit. The maximum overpressure and the arrival of the shock wave are important for two reasons; 1) insult to the first wall and any optical apertures or sensors present and 2) considerations for chamber clearing of gas or target injection through gas. The challenges of target injection have been studied[21] and the results of a study concerning chamber clearing will be published at a later date[22]. Important values of engineering interest are tabulated in Table II. Each distinct case shows a clear tread that both the overpressure for the chamber and the first wall temperature decrease with increasing radius. This is expected as the temperature depends on the amount of x-ray attenuation that occurs but is also heavily dependent on the amount of area the heat flux is incident on. This dependence is shown in Figure 8 as the values of the first wall temperature are shown to be dependant on a $1/r^2$ relation with a high confidence level (the fit has R^2 of 0.9998). This is also seen in the

overpressure, which is dependent on the overall volume of the gas behind the blast wave, as the pressure depends on the force of the blast wave distributed about the surface of the first wall. The relation of this then is dependent on a $1/r^3$ relation with a high confidence as shown in Figure 9 (here the R^2 value is 0.9758). These relations are seen for all the gas fill and densities performed in the parameter study.

V Discussion

The BUCKY simulations show a trend that was expected: As the chamber radius increases both the first wall temperature and the overpressure decrease. The chamber gas fill and density shows the dependence of first wall heating on the prompt target x-rays; the more the gas is able to attenuate the x-ray spectra the more the first wall heating is due to the re-radiation of the chamber gas to the first wall. In all the 6 μg/cm^3 Xe chambers the maximum temperature is due to the re-radiation of x-rays onto the first wall from the gas while for the 1.83 μg/cm^3 Ar chambers the maximum temperature is due to the prompt target x-ray deposition in the first wall. The 2 μg/cm^3 Xe and 6 μg/cm^3 Ar chambers have the same result that the prompt target x-rays are the major contributor to the maximum temperature rise for all chambers of 8 m radius and less (see Figure 11 and Table II for details). This dominance of the temperature rise due to prompt x-ray emission instead of temperature rise being due to re-radiation is due the lessened impact of x-ray

attenuation. Argon has a lower opacity than the xenon, leading to less x-ray attenuation, and the lower density xenon also has a lower attenuation of x-rays when compared to the higher density cases. This influence of the density is also seen in the shock times in Table III where the high density cases lead to a longer shock propagation time as it requires more energy for the shock to reach the wall. The higher density also, as anticipated, yield a higher overpressure incident on the first wall, although in all cases the overpressure is still low. This result allows for better understanding of the exact insult to the first wall. The analytic fits to the maximum first wall temperature rise allow for limits to be placed on both the minimum and maximum size of the chamber as a small chamber allows for too much first wall heating which could have adverse affects on the integrity of the engine chamber and a large chamber has the problem of adverse engineering issues and economics. While these results are for a representative stainless steel, the analysis gives a good approximation to first wall temperature insult. The overpressure analysis shows that a pressure shock wave will not be as important in chamber engineering as the first wall temperature but does give an idea of the insult to any sensors, diagnostic tools or optical apertures that are built into the chamber walls. This insult will be nearly negligible as the reported overpressure is extremely small, and the shock arrival time will not interfere with any chamber clearing or target injection.

VI Future Work

Future studies of the engine include a similar parameter study using gas mixtures of Ar, Xe and other gases to determine whether an optimum mixture exists that minimizes the prompt temperature rise and the later temperature rise from the re-radiating gas. A non-local thermodynamic equilibrium code will be used to study the influence of non-LTE radiation physics on the chamber dynamics. Alternative first wall materials with superior thermal properties will be studied if there is a desire to reduce the chamber radius.

Acknowledgments

This work was performed under the auspices of the Lawrence Livermore National Security, LLC, (LLNS) under Contract No. DE-AC52-07NA27344 under subcontract with the University of Wisconsin, Madison.

References

[1] R.W. MOIR, "HYLIFE-II Inertial Confinement Fusion Reactor Design", *Fusion Sci. Tech.* **19** 3P2A, 617 (1991)

[2] R.W. MOIR *et al.*, "HYLIFE-II: A Molten-Salt Inertial Fusion Energy Power Plant Design-Final Report", *Fusion Sci. Tech.* **25**, 5 (1994)

[3] D. BOHNE *et al.*, "HIBALL-A conceptual design study of a heavy-ion driven inertial confinement fusion power plant", *Nuc. Eng. Des.* **73**, 195 (1982)

[4] S.I. ABDEL-KHALIK *et al.*, "Engineering Problems of Laser-Driven Fusion Reactors", *Nucl. Tech.* **43**, 5 (1979)

[5] R.F. BOURQUE *et al.*, "Overview of the Osiris IFE Reactor Conceptual Design", *Fusion Tech.* **21**, 1465 (1992)

[6] I.N. SVIATOSLAVSKY *et al.*, "A KrF Laser Driven Inertial Fusion Reactor "SOMBRERO"" *Fusion Tech.* **21**, 1470 (1992)

[7] J.D. SETHIAN *et al.*, "The Science and Technologies for Fusion Energy with Lasers and Direct-Drive Targets" *IEEE Trans. Plas. Sci.* **38**, 690 (2010)

[8] J.F. LATKOWSKI *et al.*, "Chamber Design for the Laser Inertial Fusion Energy (LIFE) Engine", *Fusion Sci. Tech.* **60**, 54 (2011)

[9] R.J. LEEPER *et al.*, "Z pinch driven inertial confinement fusion target physics research at Sandia National Laboratories", *Nuc. Fusion* **39**, 1283 (1999)

[10] M. DUNNE, "Timely Delivery of Laser Inertial Fusion Energy (LIFE)", *Fusion Sci. Tech.* **60**, 19 (2011)

[11] Private communications with V. Tang, LLNL, (2012)

[12] R.R. PETERSON *et al.*, "Inertial fusion energy target output and chamber response: Calculations and experiments", *Phys. of Plasmas* **9**, 2287 (2002)

[13] S.C. WILKS *et al.*, "Evaluation of Several Issues Concerning Laser Beam Propagation Through the LIFE Target Chamber", *Fusion Sci. Tech.* **89**, 652 (2009)

[14] K.J. KRAMER *et al.*, "Neutron Transport and Nuclear Burnup Analysis for the Laser Inertial Confinement Fusion-Fission Energy (LIFE) Engine", *Fusion Sci. Tech.* **56**, 625 (2009)

[15] G.F. KNOLL, *Radiation Detection and Measurement, 4^{th} Edition*, John Wiley & Sons, Hoboken, NJ

[16] J. YUAN and G.A. MOSES, "YAC: A code using the detailed term accounting model for all Z elements", *J.Q.S.R.T.* **99**, 697 (2006)

[17] J.J. MACFARLANE, "IONMIX-a code for computing the equation of state and radiative properties of LTE and non-LTE plasmas", *Computer Phys. Comm.*, **56**, (1989)

[18] T. HELTEMES and G.A. MOSES, "BADGER v1.0: A Fortran equation of state library", *Computer Phys. Comm.* **183**, 2629 (2012)

[19] R.M. HUNT *et al.*, "Fatigue cracking of a bare steel first wall in an inertial confinement fusion chamber", *Fusion Eng. Des.* **88**, 311 (2013)

[20] AK Steel Corp., 409 Stainless Steel Product Data Bulletin, 409-B-08-01-07, (2007)

[21] R. MILES *et al.*, "Challenges surrounding the Injection and Arrival of Targets at LIFE Fusion Chamber Centers", *Fusion Eng. Des.* **60**, 61 (2011)

[22] Private communications with Carlos Pantano, University of Illinois at Urbana-Champaign, (2014)

Fig. 1

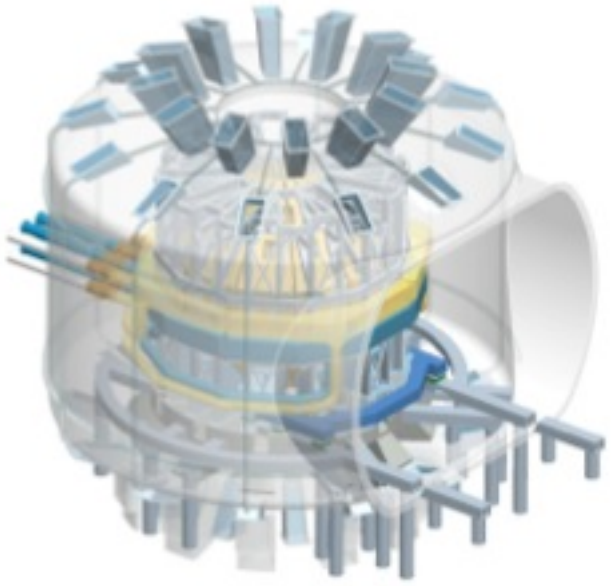

Fig. 2

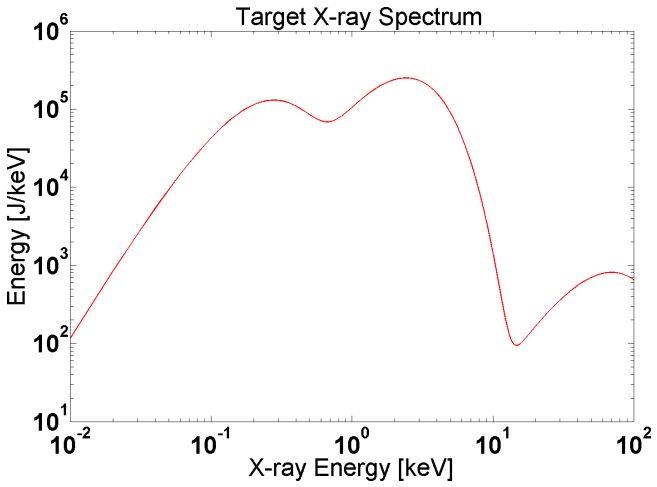
Target X-ray Spectrum
Energy [J/keV]
X-ray Energy [keV]
10^6
10^5
10^4
10^3
10^2
10^1
10^-2
10^-1
10^0
10^1
10^2

Fig. 3

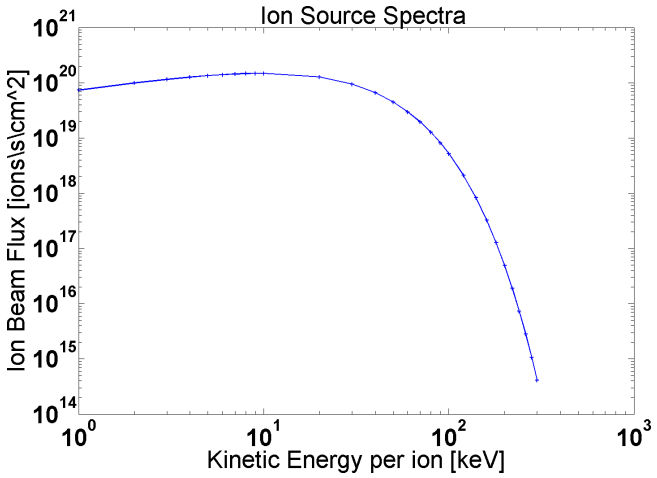
Ion Source Spectra
Ion Beam Flux [ions\s\cm^2]
Kinetic Energy per ion [keV]
10^21
10^20
10^19
10^18
10^17
10^16
10^15
10^14
10^0
10^1
10^2
10^3

Fig. 4

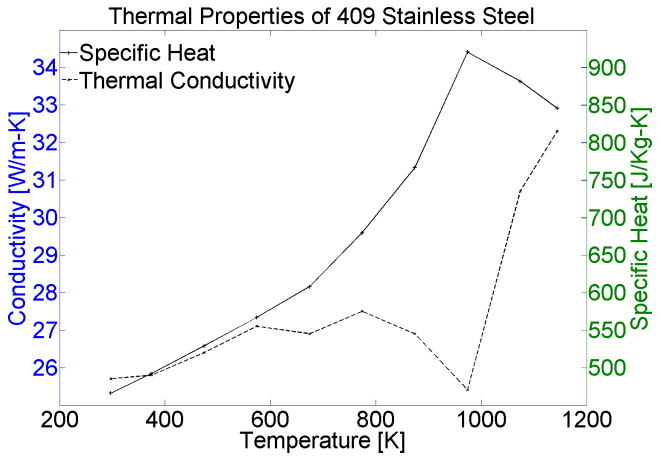
Thermal Properties of 409 Stainless Steel
Specific Heat
Thermal Conductivity
Conductivity [W/m-K]
Specific Heat [J/Kg-K]
Temperature [K]
34
33
32
31
30
29
28
27
26
900
850
800
750
700
650
600
550
500
200
400
600
800
1000
1200

Fig. 5

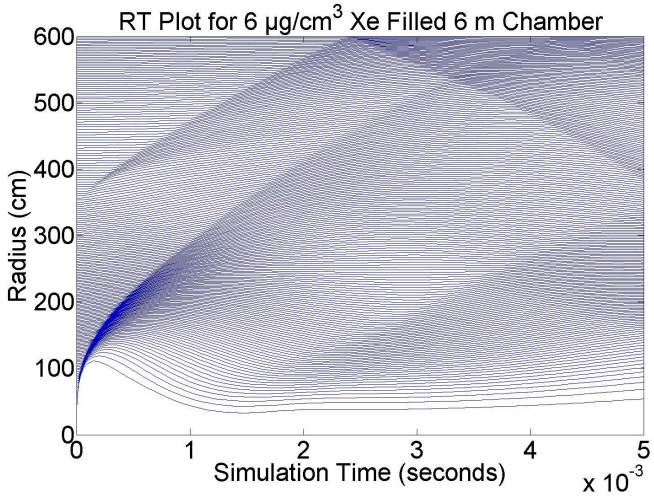
RT Plot for 6 μg/cm3 Xe Filled 6 m Chamber
Radius (cm)
600
500
400
300
200
100
0
0
1
2
3
4
5
Simulation Time (seconds)
x 10-3

Fig. 6

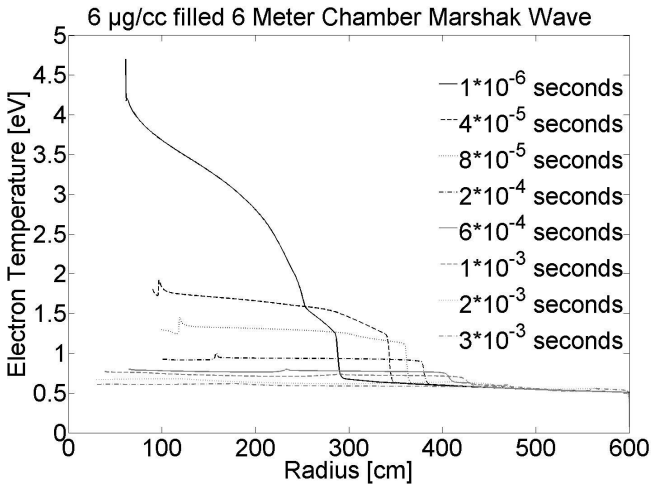
6 µg/cc filled 6 Meter Chamber Marshak Wave
Electron Temperature [eV]
Radius [cm]
1*10-6 seconds
4*10-5 seconds
8*10-5 seconds
2*10-4 seconds
6*10-4 seconds
1*10-3 seconds
2*10-3 seconds
3*10-3 seconds
0
0.5
1
1.5
2
2.5
3
3.5
4
4.5
5
0
100
200
300
400
500
600

Fig. 7

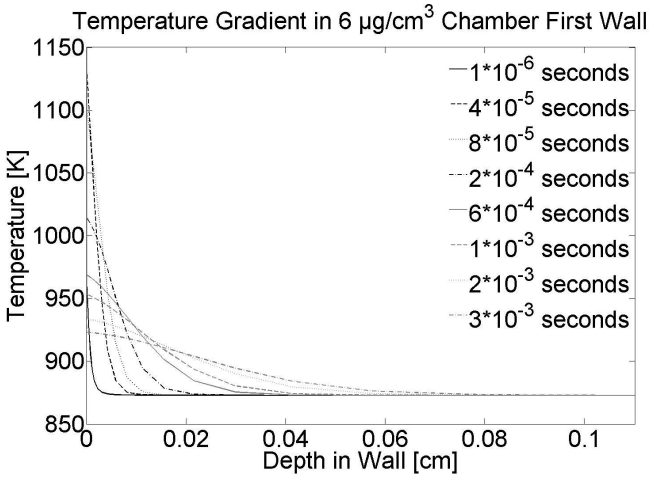
Temperature Gradient in 6 μg/cm3 Chamber First Wall
Temperature [K]
Depth in Wall [cm]
1150
1100
1050
1000
950
900
850
0
0.02
0.04
0.06
0.08
0.1
1*10-6 seconds
4*10-5 seconds
8*10-5 seconds
2*10-4 seconds
6*10-4 seconds
1*10-3 seconds
2*10-3 seconds
3*10-3 seconds

Fig. 8

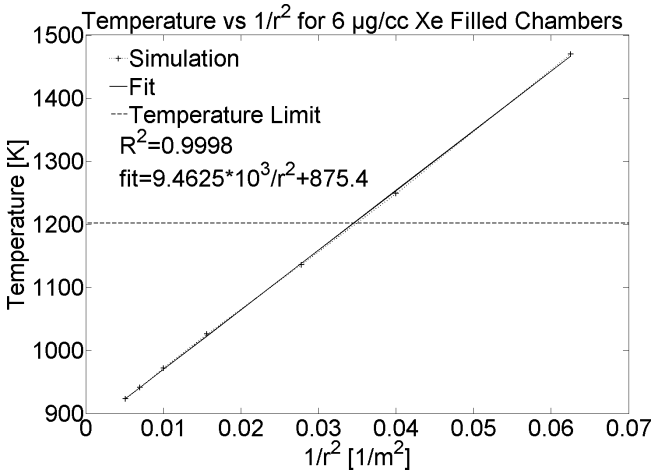
Temperature vs 1/r2 for 6 µg/cc Xe Filled Chambers
Simulation
Fit
Temperature Limit
R2=0.9998
fit=9.4625*103/r2+875.4
Temperature [K]
1/r2 [1/m2]
1500
1400
1300
1200
1100
1000
900
0
0.01
0.02
0.03
0.04
0.05
0.06
0.07

Fig. 9

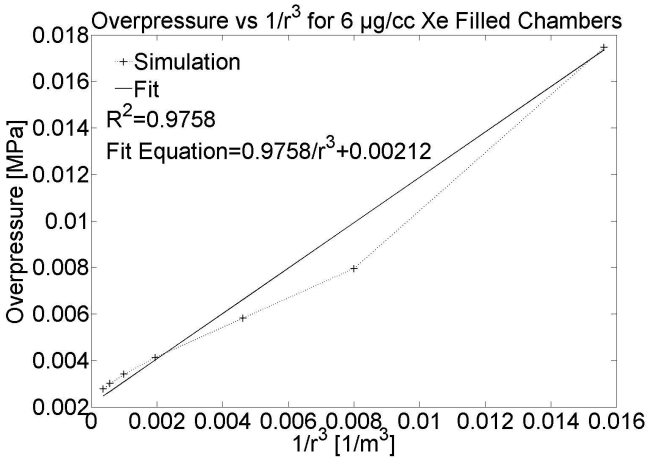
Overpressure vs 1/r^3 for 6 µg/cc Xe Filled Chambers
Simulation
Fit
R^2=0.9758
Fit Equation=0.9758/r^3+0.00212
Overpressure [MPa]
1/r^3 [1/m^3]
0.018
0.016
0.014
0.012
0.01
0.008
0.006
0.004
0.002
0
0.002
0.004
0.006
0.008
0.01
0.012
0.014
0.016

Fig. 10

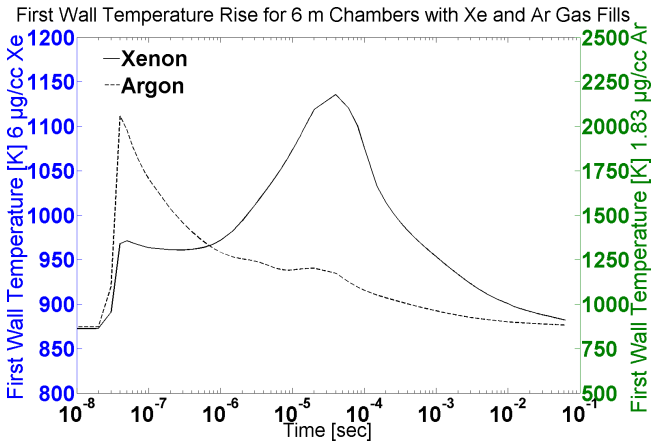
First Wall Temperature Rise for 6 m Chambers with Xe and Ar Gas Fills
Xenon
Argon
First Wall Temperature [K] 6 µg/cc Xe
First Wall Temperature [K] 1.83 µg/cc Ar
1200
1150
1100
1050
1000
950
900
850
800
2500
2250
2000
1750
1500
1250
1000
750
500
10^-8
10^-7
10^-6
10^-5
10^-4
10^-3
10^-2
10^-1
Time [sec]

Fig. 11

TABLE I

Gas Fill	6 μg/cm^3 xenon
Gas Zoning	400 Gas Zones, first 300 zones are allowed to increase by 1.3% last 100 are equal mass
Wall Zoning	70 Wall Zones, first 30 zones are 7×10^{-8} cm wide last 40 are allowed to increase by 38.5%
Chamber Radius	6 m
Wall Material	AK 409 Stainless Steel
Initial Xenon Temperature	Gas: 0.45 eV Wall: 0.0752 eV
Initial Electron Temperature	Gas: 0.45 eV Wall: 0.0752 eV
Initial Radiation Temperature	Gas: 0.0752 eV Wall: 0.0752 eV
Total Indirect Drive Target Yield Energy in Neutrons Energy in Ions Energy in X-rays	132 MJ 97.68 MJ 17.16 MJ 17.16 MJ
Opacity Data	121 logarithmically spaced FAC
EOS Data	1-T FAC Data for Xenon and 1-T BADGER[18] for steel
Minimum Time Step for x-ray Deposition	1×10^{-13} seconds
Repetition Rate	16 Hz
Laser Type	Diode pumped lasers with 351 nm wavelength
Total Laser Energy	2.2 MJ

TABLE II

Gas Type and Density	Radius	1st Wall Temperature [K]	Δt to Maximum Temperature [sec]
Xenon $6\mu g/cm^3$	4^*	1470	4.0×10^{-5}
	5^*	1249	4.0×10^{-5}
	6^*	1136	4.0×10^{-5}
	8^*	1026	4.0×10^{-5}
	10^*	972	4.0×10^{-5}
	12^*	941	4.0×10^{-5}
	14^*	923	4.0×10^{-5}
Xenon $2\mu g/cm^3$	6^+	1316	4.0×10^{-8}
	8^*	1078	1.45×10^{-5}
	10^*	1006	1.45×10^{-5}
	12^*	964	1.45×10^{-5}
	14^*	938	1.45×10^{-5}
Argon $6\mu g/cm^3$	4^+	2312	4×10^{-8}
	5^+	1600	4×10^{-8}
	6^+	1279	4×10^{-8}
	8^+	1031	4×10^{-8}
	10^*	955	4×10^{-5}
	12^*	929	4×10^{-5}
	14^*	913	4×10^{-5}
Argon $1.83\mu g/cm^3$	6^+	2057	4×10^{-8}
	8^+	1418	4×10^{-8}
	10^+	1164	4×10^{-8}
	12^+	1046	4×10^{-8}
	14^+	985	4×10^{-8}

TABLE III

Gas Type and Density	Radius	Overpressure [MPa]	Shock Arrival Time [msec]
Xenon $6\mu g/cm^3$	4	1.75×10^{-2}	0.344
	5	7.96×10^{-3}	1.31
	6	5.83×10^{-3}	2.41
	8	4.13×10^{-3}	4.80
	10	3.41×10^{-3}	7.35
	12	3.01×10^{-3}	9.97
	14	2.77×10^{-3}	12.7
Xenon $2\mu g/cm^3$	6	4.34×10^{-3}	0.622
	8	2.10×10^{-3}	2.71
	10	1.51×10^{-3}	5.08
	12	1.26×10^{-3}	7.63
	14	1.10×10^{-3}	10.3
Argon $6\mu g/cm^3$	4	2.44×10^{-2}	0.839
	5	1.80×10^{-2}	1.41
	6	1.50×10^{-2}	2.25
	8	1.20×10^{-2}	3.24
	10	1.04×10^{-2}	4.56
	12	9.60×10^{-3}	5.92
	14	9.00×10^{-3}	7.32
Argon $1.83\mu g/cm^3$	6	5.52×10^{-3}	1.46
	8	3.95×10^{-3}	2.70
	10	3.33×10^{-3}	3.50
	12	2.97×10^{-3}	5.35
	14	2.75×10^{-3}	6.75

TABLE IV

Gas Type and Density	Fit (radius r is in m)	R^2 value
Xenon $6\mu g/cm^3$	Temperature [K]: $y = \frac{9.46\times10^3}{r^2} + 875$	0.9998
	Overpressure [MPa]: $y = \frac{0.976}{r^3} + 0.002$	0.9758
Xenon $2\mu g/cm^3$	Temperature [K]: $y = \frac{1.66\times10^4}{r^2} + 843$	0.9905
	Overpressure [MPa]: $y = \frac{0.760}{r^3} + 0.0008$	0.9956
Argon $6\mu g/cm^3$	Temperature [K]: $y = \frac{2.42\times10^4}{r^2} + 709$	0.9768
	Overpressure: $y = \frac{0.990}{r^3} + 0.009$	0.9852
Argon $1.83\mu g/cm^3$	Temperature [K]: $y = \frac{4.78\times10^4}{r^2} + 709$	0.9955
	Overpressure [MPa]: $y = \frac{0.636}{r^3} + 0.003$	0.9948

Fig. 1. Conceptual depiction of the engine chamber. The radius of the chamber and the fill gas are varied in the simulations of this paper, though the standard design calls for 6 meter radius.

Fig. 2. Conceptual design of the engine chamber sealed within an outer vacuum chamber.

Fig. 3. X-ray spectrum point source for the simulations. The spectrum is normalized to 1 MJ and then scaled to the desired x-ray yield.

Fig. 4. Ion spectrum point source for the simulations. This spectrum is scaled to the desired ion yield.

Fig. 5. Thermal properties for the steel first wall material. The specific heat is solid and the thermal conductivity is dashed.

Fig. 6. Radius-Time plot for the base case of 6 μg/cm^3 of xenon in a 6 meter chamber. The plot shows the arrival of two shock waves, with the outer shock reaching the wall at 2.7 ms and the inner shock at 4.5 ms.

Fig. 7. Marshak wave propagation for the 6 meter 6 μg/cm^3 xenon filled chamber. The wave begins to slow the further it propagates out, with the front speed dropping sharply at approximately 100 μs at a radius around 330 cm, which is the same radius where the outer shock develops.

Fig. 8. Temperature gradient in the first wall of the 6 μg/cm^3 xenon filled 6 meter chamber. The gradient is steep as the first wall heats initially and then decreases as the heat diffuses through the wall.

Fig. 9. Fit (solid) vs simulation results (dot) for the 6

μg/cm^3 Xe chamber first wall temperature vs. radius. The 4 and 5 meter cases have temperatures above the safety limit.

Fig. 10. Fit (solid) vs simulation results (dot) for the 6 μg/cm^3 Xe chamber overpressure vs. radius.

Fig. 11. Comparison of 6 meter chambers with 1.83 μg/cm^3 Ar (dashed) and 6 μg/cm^3 Xe (solid) gas fills. The Ar chamber has a maximum temperature rise due to the prompt x-ray release while the Xe chamber has a maximum temperature rise due to thermal transport from the chamber gas into the first wall.

TABLE I. Simulation Parameters for Base Case

TABLE II. First Wall Temperature Load and Time to Maximum Temperature

Note: All chambers with * next to the radius have maximum temperature due to heating from re-radiating gas whereas those with $^+$ are due to heating via prompt target x-rays.

TABLE III. Maximum Overpressure on First Wall and Shock Wave Arrival Time

TABLE IV. Fits for temperature in the wall and overpressure incident on wall